ELSEVIER

Coordination Chemistry Reviews
171 (1998) 221–243

COORDINATION CHEMISTRY REVIEWS

Luminescent transition-metal-containing cyclophanes ("molecular squares"): covalent self-assembly, host–guest studies and preliminary nanoporous materials applications

Robert V. Slone, Kurt D. Benkstein, Suzanne Bélanger, Joseph T. Hupp [a], Ilia A. Guzei [b], Arnold L. Rheingold [b]

[a] *Department of Chemistry and Materials Research Center, Northwestern University, Evanston, IL 60093, USA*

[b] *Department of Chemistry and Biochemistry, University of Delaware, Newark, DE 19716, USA*

Received 28 July 1997; received in revised form 30 August 1997; accepted 19 November 1997

Contents

Abstract

An overview is given of the synthesis and characterization of a family of transition-metal cyclophanes containing rhenium tricarbonyl chloro corners and bridging diimine edges. The

PII S0010-8545(98)00031-9

synthesis of both heterometallic (Re_2M_2, M = Pd, Pt) and homometallic (Re_4) cyclophanes is described. Also briefly described are studies aimed at shedding light on the probable mechanism of high-yield assembly of homometallic molecular squares. The use of these cavity-containing assemblies as hosts in the condensed-phase binding of selected molecular guests is discussed. Also described are preliminary applications of the compounds as thin film nanoporous sensing elements. These studies suggest that the compounds may prove useful in mass-responsive or light-responsive volatile organic chemical sensing devices. © 1998 Elsevier Science S.A.

Keywords: Molecular square; Luminescence; Covalent self-assembly; Host–guest complexation; Inorganic cyclophane; Nanoporous materials

1. Introduction

Rigid macrocycles based on cis bridging ligation of transition-metals represent an unusual, and largely new, class of compounds having tremendous promise in host–guest, inclusion, and molecular recognition chemistry [1,2]. Most of the available systems are derived from Pd(II) or Pt(II) triflate species, tetranuclear with respect to metal content, and therefore arranged in square or box-like geometries, with metal atoms defining the corners [3–14]. Described in this paper is a simple, but potentially very useful, variant and extension of this theme: incorporation of visible-light-addressable, luminescent rhenium–imine, rhenium–azine or porphyrin components within a square assembly [15–17]. Induction of photoluminescent characteristics is particularly attractive in the context of eventual molecular sensing applications because it suggests an alternative to ^{1}H NMR spectroscopy for detection of guest inclusion [18,19]. Induction of luminescence also opens up the possibility of electronic excited state reactivity and manipulation of reactivity by encapsulated guests. Summarized here are both new and recently published examples.

One of the more curious — and useful — general features of the tetra-rhenium cyclophane chemistry is the very high synthetic efficiency. We present data from new experiments designed to shed light on this fortunate anomaly. Briefly, the new results lend support to earlier suggestions that the squares are formed via a thermodynamically favored covalent self-assembly mechanism.

Finally, extension of the metallocyclophane chemistry to the solid state is considered. The available data indicate that metallocyclophane-derived thin film materials are nanoporous. Some potential technological uses of the nanoporosity characteristics are outlined, and some preliminary strategies for possible volatile organic chemical sensor device development are presented.

2. Molecular synthesis

2.1. Neutral homometallic (Re_4) squares

A series of luminescent homometallic molecular squares with octahedral rhenium corners has been assembled by using $Re(CO)_5Cl$ as a starting material [16]. The

extant squares range in size from ca. 3 Å cavity length (μ-pyrazine square) to ~20 Å (edge length) for μ-5,15-dipyridyl porphyrin complexes. Apparently, the limits of this technique with respect to square cavity size have not yet been reached. The single requirement to obtain molecular squares with rhenium corners appears to be that the bridging ligand be rigid with imine or azine nitrogens oriented at 180° to each other. When a flexible ligand is used instead, dimers are often obtained. Homometallic squares have been formed in nearly quantitative yield in one step by combining the rhenium complex with an appropriate bridging ligand (such as pyrazine or 4,4-bipyridine) in a one-to-one stoichiometry. In a typical synthesis, the solution is refluxed in 4:1 tetrahydrofuran (THF):toluene under nitrogen. After ~2 days, the product precipitates and can be isolated by suction filtration. Yields in excess of 90% of analytically pure product are common for these syntheses. Six different types of homometallic molecular squares have been constructed containing edges composed of pyrazine (**1**), 4,4′-bipyridine (**2**), 1,2-bis(4-pyridyl)ethylene (**3**), 1,4-phenyl-bis(picolinoate) (**4**), 2,8,12,18-tetrabutyl-3,7,13,17-tetramethyl-5,15-(4-pyridyl)H_2-porphyrin (**5**), and 2,8,12,18-tetrabutyl-3,7,13,17-tetramethyl-5,15-(4-pyridyl)Zn(II) porphyrin (**6**). Many different isomeric forms of the molecular squares can be formed with respect to the position of the chloro ligand perpendicular to the square framework. Consequently, no general claims are made as to the isomeric composition of these compounds with respect to this ligand. We have

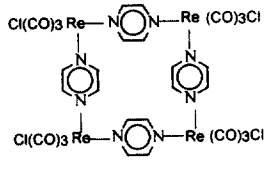

1

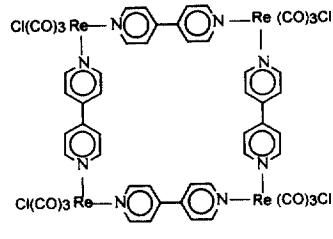

2

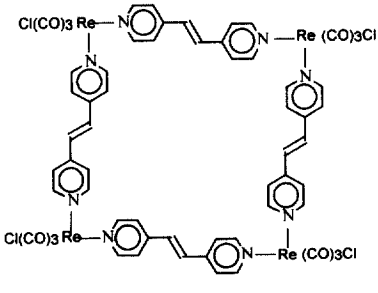

3

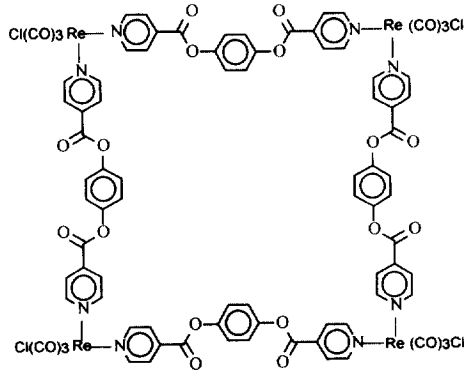

4

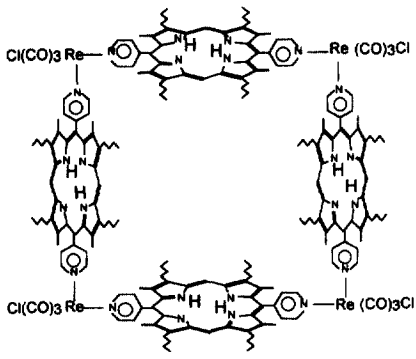

5

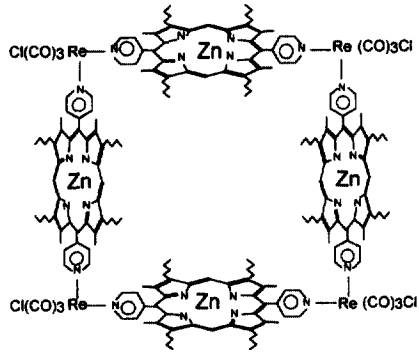

6

recently observed, however, that single-isomer metallocyclophane samples can sometimes be isolated and crystallographically characterized.

A structurally analogous set of "corner" molecules of the general formula *fac*-$Re(CO)_3(L)_2Cl$ has been synthesized using the technique of Wrighton and Giordano [20]. This set provides a context for understanding the photophysical behavior of the corresponding rhenium cyclophane assemblies. The specific molecules synthesized were: $Re(CO)_3(pyrazine)_2Cl$ (**7**), $Re(CO)_3(4,4'\text{-bipyridine})_2Cl$ (**8**), and $Re(CO)_3(phenyl\ picolinoate)_2Cl$ (**9**). (Note that in complex **9**, a proton takes the place of the second picolinoate moiety of square **4**.)

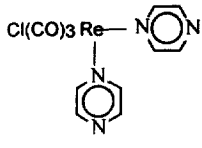

7

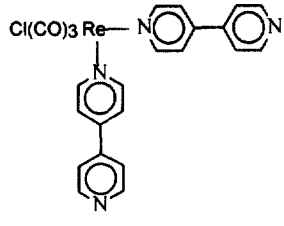

8

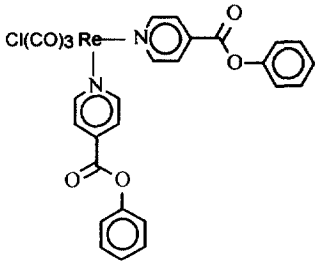

9

2.2. Charged heterometallic (Re_2M_2) squares

Additionally, a set of heterometallic molecular squares has been constructed. For example, $Re(CO)_3(4,4'\text{-bipyridine})_2Cl$ [20] and $Pd(OTf)_2(dppp)$ [21–23] (OTf = trifluoromethanesulfonate, dppp = diphenylphosphinopropane) have been combined in 1:1 stoichiometry in methylene chloride to create a luminescent Re_2Pd_2 square (**10**; alternating Re and Pd corners) [15]. The platinum derivative (**11**) has recently been synthesized as well by substituting $Pt(OTf)_2(dppp)$ for palladium. This synthesis yields the square in roughly 80% yield. The properties of the Re_2Pd_2 molecular square have been described previously [15]. As indicated in part below, the substitu-

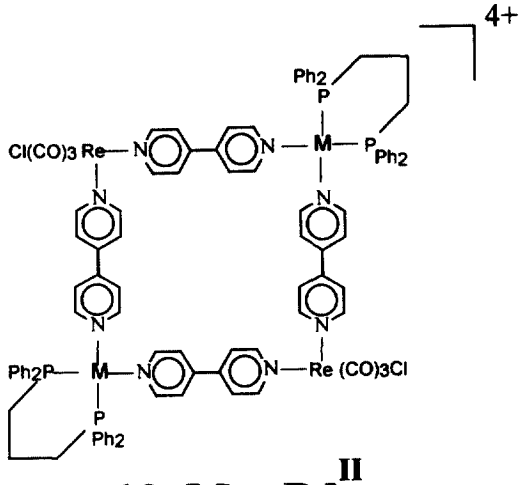

10 M = Pd^{II}

11 M = Pt^{II}

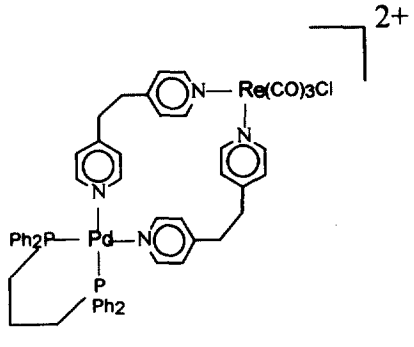

12

tion of Pt(II) for Pd(II) apparently has little effect upon the majority of the critical properties of the complex.

X-ray quality crystals of square **10** were grown by layering an acetonitrile solution of the complex with benzene [24]. The structural data (Tables 1 and 2 and Fig. 1)

Table 1
Crystallographic information for **10**

Chemical formula	$Re_2Pd_2C_{160}H_{144}N_{12}O_{18}F_{12}P_4S_4Cl_2$	
Formula weight	3659.09	
Temperature (K)	223(2)	
Crystal system	Triclinic	
Space group	$\bar{P}$	
Unit cell dimensions	$a=12.4729(2)$ Å	$\alpha=86.7910(10)^\circ$
	$b=17.0561(2)$ Å	$\beta=87.1100(10)^\circ$
	$c=19.4246(2)$ Å	$\gamma=77.5910(10)^\circ$
Volume (Å^3), Z	4026.38(9), 1	
Density (calc.) (mg/m^3)	1.509	
μ (Mo Kα) (mm^{-1})	1.923	
Crystal size (mm^3)	$0.30\times0.15\times0.06$	
Color, habit	Yellow, blade	
Reflections collected	26 814	
Independent reflections	17 312 ($R_{int}=0.0373$)	
Absorption correction	Empirical	
T_{max}/T_{min}	1.000/0.796	
Refinement method	Full-matrix least-squares on F^2	
Diffractometer	Siemens P4/CCD	
Goodness-of-fit on F^2	1.027	
$R(F)$ (%)[a]	7.20	
$R(wF^2)$ (%)[a]	16.35	
Largest difference peak and hole (e Å^{-3})	2.358 and −2.424	

[a] Quantity minimized is $R(wF^2)=\Sigma[w(F_o^2-F_c^2)^2]/\Sigma[(wF_o^2)^2]^{1/2}$; $R=\Sigma\Delta/\Sigma(F_o)$, $\Delta=|(F_o-F_c)|$.

Table 2
X-ray structural data for **10**

Selected bond lengths (Å)		Selected bond angles (°)	
Pd1–P1	2.282(1)	N2–Pd1–N3	86.1(2)
Pd1–P2	2.279(2)	P1–Pd1–P2	90.8(8)
Pd1–N2	2.109(6)	N2–Pd1–P2	93.1(2)
Pd1–N3	2.111(6)	P1–Pd1–N3	90.0(2)
Re1–Cl1	2.451(6)	N1–Re1–N4	84.6(2)
Re1–N1	2.216(6)	N1–Re1–C2	95.2(3)
Re1–N4	2.231(6)	C2–Re1–C3	90.4(3)
Re1–C1	2.117(13)	Cl1–Re1–C1	176.6(4)
Re1–C2	1.926(10)	Cl1–Re1–N1	87.1(2)
Re1–C3	1.921(8)		
Re1–Pd1	11.363(13)	4,4′-bpy torsion	37.3(3)

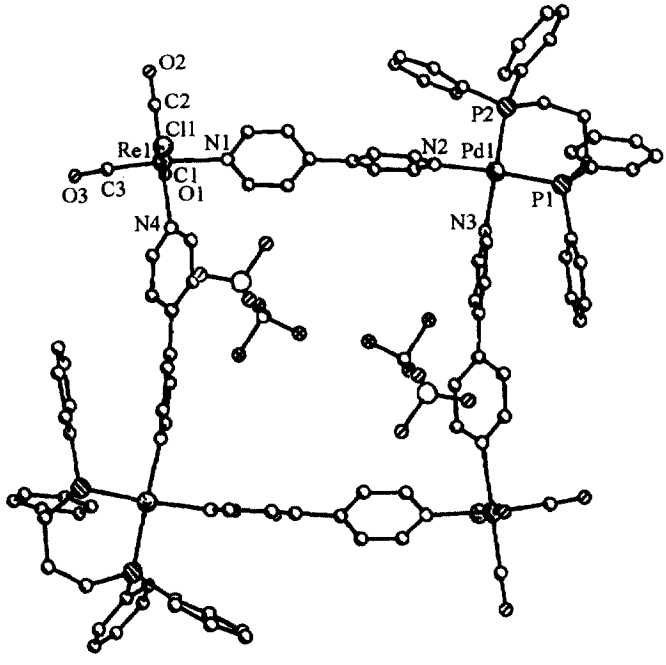

Fig. 1. Single crystal X-ray structure of square **10**.

reveal a slight distortion from a strictly square cavity geometry [i.e. angles of 86.0° about the Pd(II) and 84.5° about the Re(I) metal centers]. These results are in accord with our earlier findings for the homometallic square structures [16]. Additionally, the phenyl rings of the diphenylphosphinopropane ligands reside directly over the neighboring pyridyl rings of the 4,4′-bipyridine. This structural feature prohibits the all-palladium and platinum phosphine squares from forming smaller cavities with edges such as pyrazine [9]. The homometallic rhenium squares, on the other hand, are capable of being tuned in size from dipyridylporphyrin down to pyrazine due to the lack of steric bulk about the rhenium metal center. Finally, it is worth noting that two of the four triflate counterions for square **10** were located within the square cavity (along with four equivalents of benzene, not shown) in the solid state. Their presence within the cavity makes the use of these small, charged palladium and platinum materials in solid state studies difficult, unlike the neutral homometallic rhenium square cyclophanes (see Section 6) which possess extended, open channels.

An attempt to extend the rhenium–palladium chemistry by replacing 4,4′-bpy with bis(4-pyridyl)ethane (**BPA**) as the bridging ligand yielded a compound (**12**) that analyzed correctly for a molecular square, but proved by FAB MS to be a dinuclear metal complex [15]. The formation of macrocyclic dinuclear metal complexes has also been noted by Fujita et al. in their studies with flexible bridging ligands [6].

Curiously, compound **12**, unlike **10**, is non-emissive at room temperature in both acetone and CH_2Cl_2.

2.3. Mechanistic studies

Typically, high dilution conditions have been required for the synthesis of cyclophane compounds [25,26]. For kinetically controlled assembly processes (i.e. irreversible assembly processes) dilution will generally statistically enhance cycle formation relative to polymer formation. The apparent lack of sensitivity of the tetra-rhenium cyclophane syntheses to concentration levels suggests that labile intermediates exist (see below) that permit eventual condensation of thermodynamic products. Also likely facilitating the high-yield assembly of metallocyclophanes are: (1) the substantial degree of preorganization provided by rigid corner complex formation, and (2) the equilibrium-shifting precipitation of product (molecular square) species.

Several studies have addressed the role of thermodynamic factors in the self-assembly of macrocycles [27–29]. They generally have concluded that: (a) cyclic structures are preferred over oligomers for enthalpic reasons, and (b) small cycles are favored over large cycles for entropic reasons. The enthalpic preference derives simply from the increased number of bonds obtainable per subunit for a cyclic structure as opposed to an oligomer. For example, the cyclic $[Re(CO)_3(\mu\text{-}4,4'\text{-bpy})Cl]_4$ structure yields 2.00 metal–nitrogen bonds per Re(4,4′-bpy) subunit while the corresponding four unit linear chain yields only 1.75 rhenium–nitrogen bonds per Re(4,4′-bpy) subunit. Based on 90° imine–metal–imine bond angles and complete ligand rigidity, the smallest accessible macrocycle is then the experimentally observed square assembly. Fujita et al. have pointed out, however, that if either criterion can be relaxed then even smaller *trimetallic* cycles can be accessed [4].

Given the apparent thermodynamic preferences we decided to investigate whether the μ-4,4′-bipyridine square would still form under less ideal conditions, i.e. bridging ligand/metal stoichiometries differing from one-to-one. It is known that with a large excess (10-fold) of bridging ligand in refluxing isooctane the monomeric complex $Re(CO)_3(4,4'\text{-bpy})_2Cl$ is obtained from $Re(CO)_5Cl$ [20]. In our mechanistic studies, a two-to-one ligand-to-metal ratio was utilized and the ligand (4,4′-bpy) and metal (rhenium) were preassembled as the corner complex, **8**. Treatment of the coordinatively unsaturated corner with refluxing THF/toluene (i.e. standard conditions for molecular square preparation) produced the corresponding square, **2**, in 74% isolated yield based on rhenium. In addition, NMR measurements of the post-workup filtrate solution indicated that significant free 4,4′-bipyridine was generated. These results clearly indicate that the nominally inert rhenium–imine complex can be thermally labilized under conventional synthesis conditions. The findings also lend support to the "thermodynamic preference" hypothesis described above.

In a second experiment, $Re(CO)_5Cl$ was refluxed simultaneously with *two* potential bridging ligands, pyrazine and 4,4′-bipyridine. Remarkably, only the molecular square assemblies, **1** and **2**, were observed as products (HPLC and ^1H NMR measurements), despite the anticipated statistical preference for 50% mixed-ligand

complex (e.g. molecular rectangle) formation. These findings likewise support the idea of a strong thermodynamic bias toward square formation, albeit for additional (unknown) reasons, since the simple arguments outlined above would also support rectangle formation. In any case, we note that a possible alternative explanation in terms of squares (as opposed to the rectangle) as kinetic products is likely inapplicable since the substitution kinetics are almost certainly governed by Re–CO bond dissociation [30,31].

Implied in each of the preceding mechanistic studies is the involvement of one or more soluble intermediates — presumably solvento complexes. If so, then the identity of the solvent could play a crucial role in the success of the synthesis. To test this idea, we attempted the synthesis of the 4,4′-bipyridine bridged square complex, **2**, in alternative media. We found that when the reaction was performed in neat toluene at 60 °C, the tetramer failed to form. When run in neat THF, however, the square did form and ultimately precipitated in greater than 90% yield. The striking reactivity differences presumably reflect the ability of THF, but not toluene, to form weak adducts with rhenium. We suggest that under these reaction conditions, the THF, which is present in large excess, may reversibly substitute for a pyridyl group, leading to a series of rhenium–pyridyl bridged structures until the tetrameric cycle is completed and precipitates from solution. The proposed scheme is similar, therefore, to that suggested by Fujita et al. for their palladium-containing square [3].

Finally, we note that related synthetic studies involving cationic palladium species often yielded catenated macrocycles [7]. In contrast, we have failed to detect catenated products in any of the rhenium-based syntheses. These interesting differences are almost certainly a consequence of solvent polarity or dispersion-energy differences. As Fujita and coworkers point out, the net positive charges of the catenate-forming palladium complexes render them soluble in high polarity solvents such as water. Aqueous solubility is typically further enhanced by including known hydrogen-bond donating ligands in the Pd(II) coordination sphere and by employing nitrate as a counter ion [3–7]. Under these conditions, solvent interactions can be minimized and dispersive interactions can be maximized by placing aromatic bridging ligands from neighboring complexes in contact, i.e. by catenate formation. In contrast, in THF/toluene as the reaction medium the "solvophobic" and ligand/ligand dispersion energy advantages of catenate formation are much less significant and catenate formation is not detected.

3. Molecular photophysics

3.1. Absorption and emission spectra

Fig. 2 shows that both corner and square complexes are near-UV chromophores. From the figure, the lowest energy absorption feature of the square complex, **2**, lies 3000 cm^{-1} below the lowest energy feature in the spectrum of the corresponding corner complex, **8** [16]. The shift is reminiscent of that observed upon ligand protonation of **8**, and is consistent with prior assignments of the feature as a predominantly metal-to-ligand charge transfer (MLCT) transition [20,32–34]. Thus,

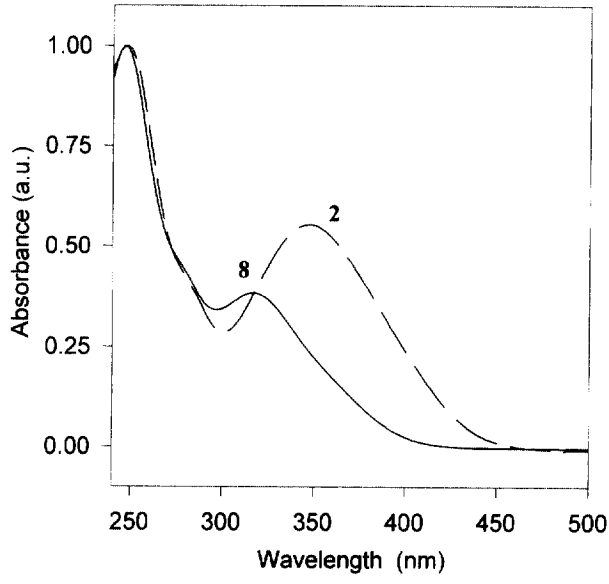

Fig. 2. Electronic absorption spectra for 1×10^{-5} M **2** (- - -) and 2.4×10^{-5} M **8** (————) in CH_2Cl_2 as solvent.

both H^+ and Re(I) should lower the MLCT excited state by electrostatically stabilizing a negative charge in the acceptor (π^* 4,4′-bpy) orbital. Photoexcitation within the nominally singlet MLCT band of either **2** or **8** results in the formation of an emissive triplet (or nominally triplet) excited state [16]. Table 3 shows that all of the available rhenium-containing cyclophanes, except the 1,2-bis(4-pyridyl)ethylene (BPE)-containing cyclophane, are detectably emissive in solution at room temper-

Table 3
Electronic absorption and luminescence properties

Complex	λ_{LIG} (nm)	λ_{MLCT} (nm)	λ^a_{em} (nm)	τ^a (ns)	E^b_{0-0} (eV)
(**1**) $[Re(CO)_3(\mu\text{-pz})Cl]_4$[d]	274	396	682	26	2.03
(**7**) $Re(CO)_3(pz)_2Cl$[d]	264	320	584	318	2.33
(**2**) $[Re(CO)_3(\mu\text{-4,4′-bpy})Cl]_4$[d]	248	348	632	134	2.17
(**8**) $Re(CO)_3(4,4'\text{-bpy})_2Cl$[d]	248	316	585	1670	2.33
(**4**) $[Re(CO)_3(\mu\text{-diester})Cl]_4$	265	338	661	63	2.08
(**9**) $Re(CO)_3(py\text{-}est\text{-}ph)_2Cl$	265	338	661	64	2.08
(**3**) $[Re(CO)_3(\mu\text{-bpe})Cl]_4$[d]	294	358	—[c]	—[c]	—[c]
(**10**) $[Re_2Pd_2(\mu\text{-bpy})_4]\cdot 4OTf$[e]	260	332	610	17	2.24
(**11**) $[Re_2Pt_2(\mu\text{-bpy})_4]\cdot 4OTf$	250	338	610	18	2.24

[a] Measured in deoxygenated CH_2Cl_2 at room temperature; λ_{em} values corrected for instrument response.
[b] E_{0-0} estimated as in ref. [15].
[c] No luminescence detected.
[d] Data from ref. [16].
[e] Data from ref. [15].

ature. The absence of emission from the BPE-containing complex is tentatively ascribed to intramolecular energy transfer to the ethylene portion of the molecule, as has previously been observed for related complexes [35].

Table 3 also summarizes the available square and corner complex absorption data. As can be seen in the table, the square complexes (with the exception of the ester square and corner which have identical photophysical properties) absorb and emit at lower energy than their corresponding corners.

3.2. Non-radiative decay rates

Lifetimes, and therefore rates of decay of emissive excited states of monomeric tricarbonyl chlororhenium imine, diimine, and azine complexes, are typically controlled by non-radiative decay kinetics [36]. From Table 3, shorter lifetimes are observed for photoexcited squares than for corners. To ascertain whether the shortening resulted from a simple increase in the non-radiative decay rate [37,38] or from a more complicated process, a global "energy gap plot" ($\ln \tau$ vs. the energy of emission, E_{em}; Fig. 3) was constructed. Included in the plot were the available luminescent squares and corners as well as several related monometallic complexes previously characterized in the literature [36,39,40]. Given the chemical variability in chromophoric ligands in the plot, exact energy gap behavior would not be expected. Nevertheless, the plot clearly shows that these complexes behave as

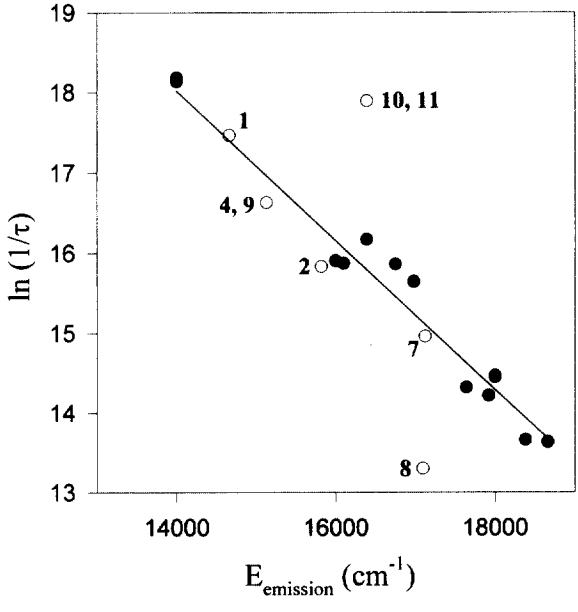

Fig. 3. Energy gap plot for molecular squares **1**, **2**, **4**, **10**, and **11**, as well as corners **7**, **8**, and **9**, and selected monometallic tricarbonylchlororhenium complexes (see refs. [39,40]). Excited state lifetime data (s) obtained in deoxygenated CH_2Cl_2 at 298 K.

expected based on a purely non-radiative control of their excited state lifetimes. The only square complexes to depart from the correlation are the heterometallic assemblies. The chemical basis for the departures is discussed in the following section.

3.3. *Intramolecular electron transfer quenching*

As shown in Fig. 4 for square **10**, heterometallic square formation, like homometallic square formation, induces significant red shifts in triplet MLCT excited state emission energies [15]. In contrast to the homometallic cases, however, heterometallic square formation also substantially decreases (ca. 25-fold) the emission intensity [15]. Time-resolved luminescence measurements (deoxygenated acetone) demonstrate that intensity losses are associated with attenuations of the excited state lifetime: $\tau(\mathbf{8}) = 645$ ns; $\tau(\mathbf{10}) = 17$ ns; $\tau(\mathbf{11}) = 18$ ns. As noted above, energy gap considerations predict shorter lifetimes for the squares than for the corresponding corners [16,37,38]. From Fig. 3, the degree of attenuation for either square complex is clearly too large to be accommodated by energy gap effects; instead the effects are attributed to quenching by ligated Pd(II) and Pt(II) fragments. Bimolecular Stern–Volmer studies [**8** with added Pd(bis-diphenylphosphinopropane)-(pyridine)$_2^{2+}$ (**13**); see Fig. 5) confirm that efficient Pd-based quenching is possible ($k_q = 3 \times 10^9\ M^{-1}\ s^{-1}$) [15]. The absence of absorption/emission spectral overlap for **13** with either **8** or **10**, however, rules out Förster energy transfer as the quenching mechanism [41].

At least for **10**, the available electrochemical and luminescence data [15] offer considerable insight into the viability of alternative electron transfer (ET) quenching

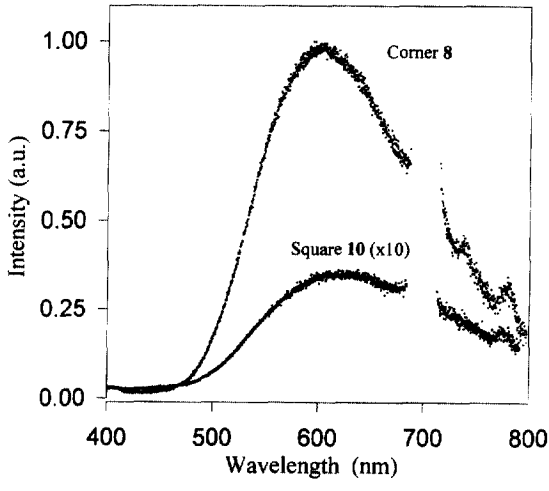

Fig. 4. Instrument response corrected emission spectra (note difference in scale) for **8** and **10** in deoxygenated CH_2Cl_2 as solvent. For both samples, the absorbance at λ_{exc} (350 nm) was 0.1. The discontinuities within both spectra at 700 nm correspond to the removal of data from the second harmonic of the 350 nm excitation.

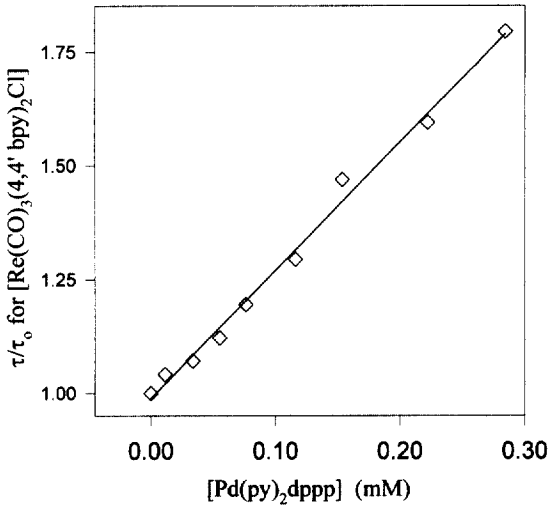

Fig. 5. Stern–Volmer addition of **13** to a solution of **8** in acetone at room temperature.

pathways. As described elsewhere [15], the potential for oxidation of photoexcited **10** is estimated as ca. −0.9 eV vs. SCE. Again as described elsewhere [15], an upper limit estimate of −0.56 V vs. SCE can be obtained for the potential of the Pd(II/I) couple. Thus the combined potential data are energetically consistent with an oxidative quenching mechanism (i.e. coordinated bipyridyl radical anion to palladium ET), with $k_{ET}=6\times10^7\ s^{-1}$ (based on the availability of two quenchers per photoexcited square). This electron transfer quenching pathway, of course, introduces an additional term in the denominator of the usual radiative quantum yield expression, thereby diminishing both the luminescence lifetime and intensity [42]. An alternative reductive quenching pathway can be discounted on the basis of the absence of a signal for the oxidation of **13** below the solvent limit.

Finally, we wish to suggest that palladium-based redox quenching may also possibly account for the otherwise puzzling photophysical behavior of some recently reported related molecular square assemblies containing porphyrin edges [14]. Most notably, no luminescence can be detected from these assemblies in fluid solution. While the possible complicity of heavy-atom effects (palladium and platinum) has been noted [14], rhenium-corner-containing porphyrin square assemblies are not strongly influenced by the presence of heavy atoms [17]. If the redox quenching explanation is correct, then it is likely that analogous platinum-corner-containing porphyrin squares would also be non-luminescent.

4. Redox energetics

4.1. Ground state potentials

The ground state electrochemistry of the tetra-rhenium cyclophanes exhibits some interesting size-dependent behavior. Shown in Table 4 are the ground state redox

Table 4
Ground state electrochemical potentials

Complex	$Re^{(I/II)}$ [a] (V)	$Ligand^{(0/1-)}$ (V)
(1) $[Re(CO)_3(\mu\text{-pz})Cl]_4$	+1.58	−0.92
		−1.23[d]
(7) $Re(CO)_3(pz)_2Cl$	+1.46	−1.51
		−1.87[d]
(2) $[Re(CO)_3(\mu\text{-4,4'-bpy})Cl]_4$	+1.35	−1.15
		−1.26[d]
(8) $Re(CO)_3(4,4'\text{-bpy})_2Cl$	+1.36	−1.57
		−1.67[d]
(9) $Re(CO)_3(py\text{-}CO_2\text{-}ph)_2Cl$ [b]	+1.40	−1.38
(6) $[Re(CO)_3(\mu\text{-ZnP})Cl]_4$	+1.37	—[c]

[a] All potentials shown are vs. SCE(aq.) in 0.1 M TEAP in acetonitrile. Scan rates were 500 mV/s in order to obtain semi-reversible behavior for $Re^{I/II}$.
[b] Due to low solubility of the diester square complex, values for the diester square potentials are estimated from the corner potentials.
[c] Values omitted because of the complicated nature of electrochemical processes occurring at negative potentials. Reversible, porphyrin-localized oxidations are observed at +0.62 V and +0.86 V.
[d] An alternate assignment is a metal-localized reduction.

potentials (cyclic voltammetry) for ligand reduction as well as metal oxidation. The latter are complicated by rapid decomposition of the resulting 17-electron Re(II) species; consequently, the reported values should be regarded as only estimates. In contrast, in the ligand reduction region the electrochemical responses are chemically reversible. For the smallest square (μ-pyrazine; 1) the successive reduction waves are separated by 310 mV. Rotating disk voltammetry measurements indicate that each reductive wave entails the addition of two electrons (assuming that the irreversible metal oxidation wave involves the loss of four electrons). Our interpretation is that electronically and electrostatically isolated pyrazine ligands on opposing edges of the molecular square are reduced first. Then, at more negative potentials, the neighboring pyrazine edges are reduced. The 4,4′-bipyridine squares display a similar, but smaller, splitting of reduction potentials for the putative opposing and adjacent bipyridines (ca. 110 mV). Qualitatively similar size-dependent behavior has been reported previously for a cyclic complex composed of ferrocene-containing subunits [43].

In the oxidative region rhenium becomes approximately 120 mV more difficult to (irreversibly) oxidize in the pyrazine square complex in comparison to the corresponding corner. With the longer, and less strongly electronically communicating, 4,4′-bipyridine ligand, replacement of the corner complex by the square complex yields almost no change in the (irreversible) Re(I/II) potential.

4.2. *Excited state potentials*

Excited state potentials for the luminescent homometallic squares and related corner complexes, as calculated from the ground state potentials and estimated

Table 5
Excited state redox potentials

	M^+/M^* (V)	M^*/M^- (V)
(**1**) $[Re(CO)_3(\mu\text{-pz})Cl]_4$	−0.45	1.11
(**7**) $Re(CO)_3(pz)_2Cl$	−0.87	0.82
(**2**) $[Re(CO)_3(\mu\text{-4,4'-bpy})Cl]_4$	−0.82	1.02
(**8**) $Re(CO)_3(4,4'\text{-bpy})_2Cl$	−0.97	0.76
(**4**) $[Re(CO)_3(\mu\text{-diester})Cl]_4$	−0.68	0.70
(**9**) $Re(CO)_3(py\text{-}CO_2\text{-}ph)_2Cl$	−0.68	0.70

All potentials are vs. SCE(aq.) in acetonitrile.

E_{0-0} values [15,44], are shown in Table 5. The values for square **4** were calculated by using the ground state potentials of corner **9** because of the low solubility of **4**.

5. Molecular host–guest behavior

5.1. Complex anion binding by a heterometallic molecular square

The tetracationic nature of the Re_2Pd_2 square (**10**) renders it receptive to complex anion uptake. Indeed, the emission intensity of **10** in acetone solution is enhanced by addition of electrolyte. Presumably, the anionic component of the electrolyte interacts coulombically with the doubly charged palladium corners of the host cavity. Studies in more polar solvents such as methanol show no significant change in luminescence intensity upon addition of the same electrolyte concentrations, consistent with the coulombic interaction. Additionally, there is no increase in luminescence intensity from the neutral corner complex, **8**, when electrolyte is added in analogous fashion. Curiously, the growth in luminescence intensity for the charged square occurs without changes in emission energetics or line shape, implying that the guest affects the luminescence quantum yield indirectly. We have argued elsewhere [15] that the enhancement effect derives from ion-binding-induced changes in intramolecular electron transfer quenching energetics (cf. Section 3.3). Indeed, anion encapsulation should preferentially stabilize the oxidized form of the quencher [Pd(II)] thereby decreasing the exothermicity of the oxidative quenching reaction and diminishing the quenching rate constant.

Binding studies were performed to determine the relative strengths of association between selected complex anions and the host cavity. The growth in luminescence intensity at 600 nm (with excitation at 350 nm) was fit to a binding expression of the form

$$I_i = I_0 + (\Delta I^* K_b^* C)/(1 + K_b^* C) \quad (1)$$

Within this expression, C is the concentration of the complex anion, K_b is the host–guest binding constant, and I_0 and ΔI are the initial luminescence intensity and the extrapolated maximum change in intensity at 600 nm, respectively. This

binding expression is valid when: (a) the guest concentration is significantly higher than the concentration of the host, and (b) the binding molecularity and stoichiometry are both 1:1 [45].

As shown in Fig. 6, the response of the tetracationic square to complex anions is a *differential* effect. That is, BF_4^-, which binds most strongly with a binding constant estimated at 6000 M^{-1}, induces the greatest growth in luminescence intensity. Triflate and perchlorate with binding constants of 3000 M^{-1} and 900 M^{-1} induce proportionately smaller responses. Note that the binding constant for BF_4^- represents only a lower limit since uptake of a second tetrafluoroborate ion (perhaps by simple ion pairing, rather than electrostatic encapsulation) occurs within the electrolyte concentration range examined.

5.2. *Porphyrin molecular square host–guest studies*

Metallation of porphyrin square **5** to create a Zn(II) metalloporphyrin cyclophane, **6**, has permitted us to study the ability of this rather large multi-macrocycle to accommodate small molecules within the cavity via ligation of pyridyl guests by the Zn(II) sites [17]. We note that related squares based on 5,10- and 5,15-substituted porphyrins have been reported by Drain and Lehn [14]. In addition, flexible alkyne-linked tetraporphyrin assemblies have been reported by Anderson et al. [46]. In the presence of appropriate guests, these can adopt complementary tub-shaped geometries.

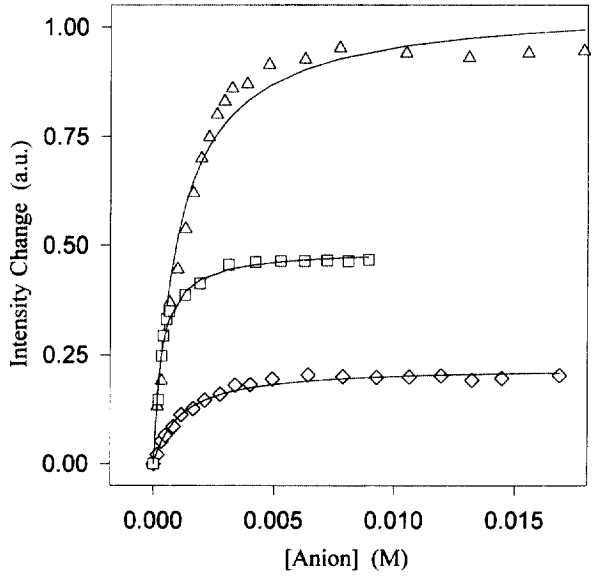

Fig. 6. Growth in luminescence intensity at E_{em} with addition of TEAP (♦), NaOTf (□), and $TEABF_4$ (△) in $\sim 1 \times 10^{-4}$ M acetone solutions of **10** at 298 K. Solid lines correspond to the binding curve fit for each complex anion.

As described in greater detail elsewhere, our initial porphyrin molecular square binding studies have centered on the use of these large, neutral complexes as hosts for dipyridyl and tetrapyridyl porphyrin guests [17]. The resulting host–guest complexes have been shown to be active with respect to energy transfer. Introduction of porphyrin-based guests typically results in nearly complete quenching of the emission intensity of the Zn(II) porphyrin host walls. In some instances the quenching of the host luminescence is accompanied by sensitization of fluorescence from the guest [17].

Studies have also been performed on multi-point binding of non-porphyritic guests. In particular, the flexible ligand bis-1,4-(4-ethylpyridyl) benzene has been used as a flexible small molecular guest which is capable of bridging between two adjacent walls of the Zn(II) metalloporphyrin square. Shown in Fig. 7 is the response of a nanomolar solution of square **6** to systematic additions of the dipyridyl guest. More than 90% of the porphyrin intensity is quenched following the addition of two equivalents of dipyridyl guest to a solution of **6** in CH_2Cl_2. The electronic absorption spectrum reveals shifts of the Soret and Q bands to longer wavelength by (ca. 10 nm; not shown) as expected for binding to the Zn(II) porphyrin portions of the host [47,48]. From Fig. 7, the binding constant for the interaction of this small ligand with the metalloporphyrin square host is $\sim 2.4 \times 10^8\ M^{-1}$.

As a control study, the same dipyridyl ligand guest was brought into contact with ZnTPP (TPP = tetraphenylporphyrin). In this case, only one end of the flexible guest can be bound by the metalloporphyrin. A lower binding constant is expected based

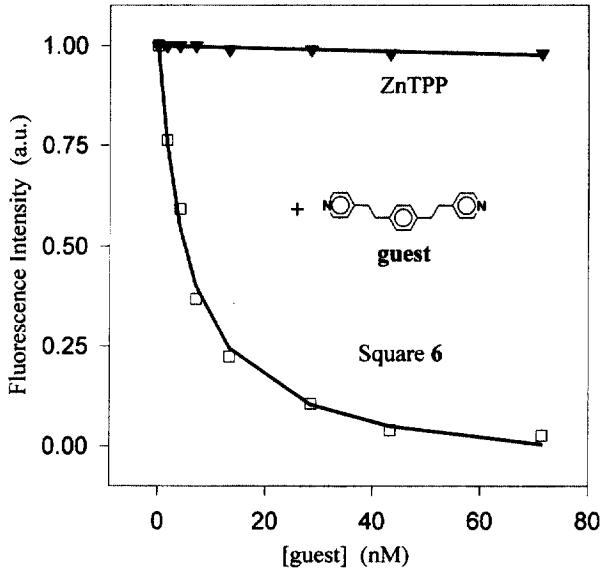

Fig. 7. Fluorescence intensity (at $\lambda_{em} = 595$ nm) of **6** (□) and ZnTPP (▽) (both at 10^{-9} M in CH_2Cl_2) with addition of dipyridyl ligand guest. Solid lines correspond to the binding curve fits for ZnTPP and square **6**.

on the ability to achieve only one stabilizing interaction per assembly. Indeed, when micromolar amounts of the dipyridyl ligand are introduced to a nanomolar solution of ZnTPP, Fig. 7, no measurable change in luminescence intensity occurs.

6. Thin film materials and applications

6.1. Nanoporosity

X-ray derived molecular structures for two of the available light-emitting tetrarhenium cyclophane complexes (**1** and **2**) have recently been reported [16]; these confirm the putative square geometries. Importantly, as illustrated in Figs. 8 and 9 for assembly **1**, the structural studies also show that: (a) squares can crystallize to form periodic porous structures {i.e. the orthogonal cavity-filling catenated structures often observed for extended (non-molecular) arrays [49–53] are not encountered here}, and (b) the pores or cavities are appropriately aligned to create semi-infinite channels. The extended channels should render the crystalline materials permeable to appropriately small molecular or ionic species. As suggested below, induction of nanometer scale porosity and permeability could have significant implications in terms of selective molecular sensing and related applications. Such applications are more readily implemented, however, with microcrystalline thin films than with macroscopic single crystals.

To determine whether the desired nanoporosity is retained when the cyclophane-

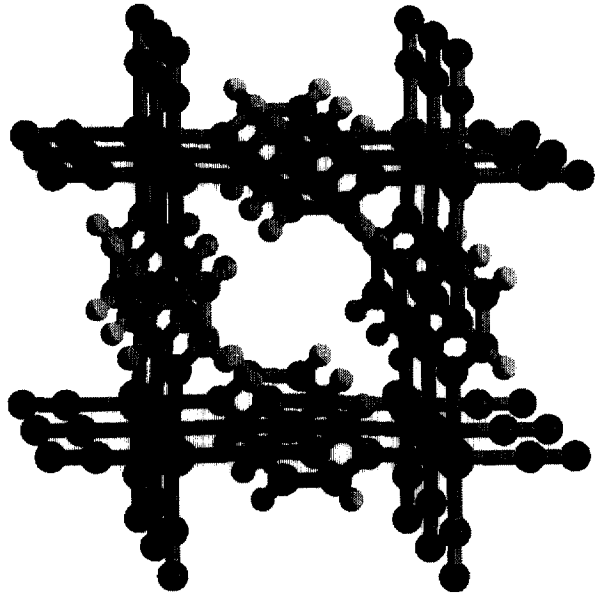

Fig. 8. X-ray crystal structure packing pattern of square **1** viewed down the major axis of a single channel.

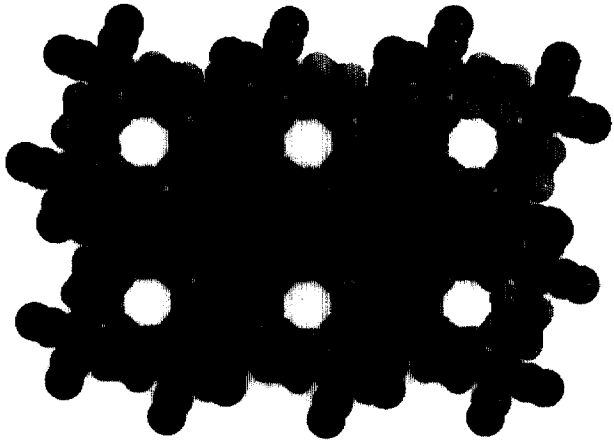

Fig. 9. X-ray crystal structure packing pattern of **1** viewed down the channel's major axis.

based materials are fabricated as thin films, we used rotating disk voltammetry as a molecular transport probe. As shown in Fig. 10, films constructed from the smallest molecular squares (**1**) proved to be permeable to the smallest available redox probe, but blocking toward larger probes. On the other hand, films constructed from squares of intermediate size (**3**) proved to be permeable to both small and intermediate sized probes, but blocking toward large probes.

6.2. *Proof-of-concept molecular sensing via microgravimetry*

Fig. 11 illustrates a preliminary experiment designed to test whether the nanoporosity of rhenium cyclophane-based films could be utilized to sense simple volatile organic compounds (VOCs) such as benzene and toluene. The sensing methodology used was a mass responsive technique, quartz crystal microgravimetry (QCM) [54–59]. Mass loading of the oscillating crystal is manifest as a decrease in oscillation frequency. As illustrated in the figure, a naked crystal is almost undetectably perturbed by exposure to toluene vapor. A crystal coated with a thin film of **2**, on the other hand, is highly responsive — consistent with uptake of toluene by the high porosity film. An additional experiment with a thin film comprised of the much smaller cyclophane, **1**, yielded a much smaller response. Since the crystographically determined cavity size for **1** is clearly too small to encapsulate toluene, we initially suspected that the residual response was associated with surface adsorption and/or guest uptake at microscopic defect sites. Further experimentation and further consideration of the available crystal structural data, however, eventually revealed that limited guest uptake was instead occurring via an interlayer inclusion mechanism. Interestingly, the available structural data indicate that uptake by interlayer inclusion is *not* possible for the corresponding rhenium–bipyridine-based material (**2**); instead, simple channel-based encapsulation is involved. Experiments presently in progress are designed to identify: (a) the key chemical and steric factors involved in high-

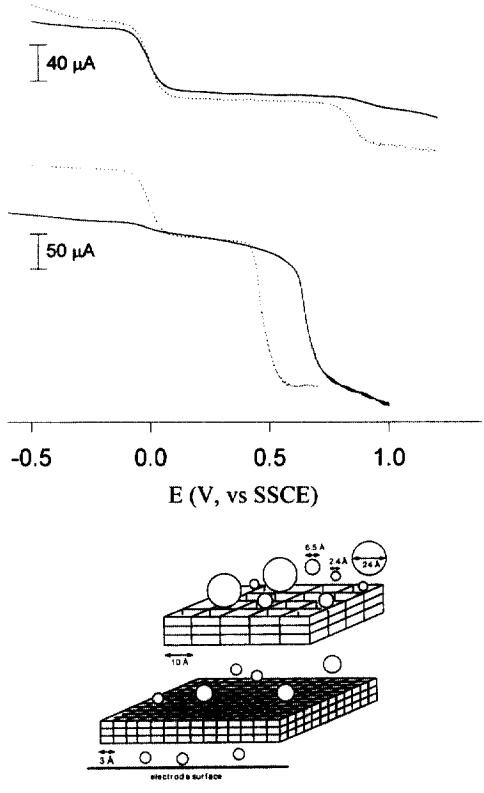

Fig. 10. Top: rotated disk electrode (RDE) voltammetry of a mixture of permeants A and B on a naked electrode (- - -) and on an electrode coated with a thin film of **3** (———). Bottom: analogous experiment performed with a mixture of permeants B and C on a thin film of **1**. Permeants A, B, and C have diameters of 24, 6.5, and 2.4 Å and oxidation potentials of ~0.9, ~0, ~0.5–0.7 V. The minimal van der Waals diameters of the molecular channels in films of **3** and **1** are ~10 and 3 Å, respectively.

affinity uptake, and (b) the detection limits achievable with the nanoporous sensing materials.

6.3. *Proof-of-concept molecular sensing via photoluminescence*

If metallocyclophane luminescence persists in nanoporous thin films, then molecular sensing should also be achievable photochemically. Panel a of Fig. 12 shows that the thin film materials indeed do photoluminesce (solid curve). Panel a also shows that the luminescence can be quantitatively quenched by exposing a film to nitrobenzene vapor (dashed curve). (QCM measurements were used to establish independently that film uptake of nitrobenzene occurs.) Panel b, on the other hand, shows that the same film is photochemically unresponsive to toluene vapor, despite the fact that toluene uptake readily occurs (see above). We attribute the behavioral differences to the ability of nitrobenzene — but not toluene — to engage in electron

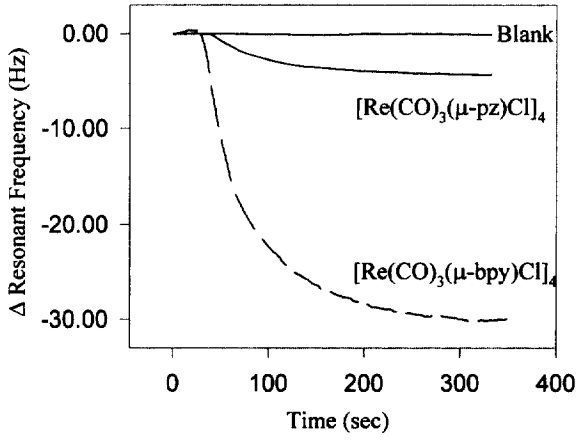

Fig. 11. Comparative QCM responses of: film of **1**, film of **2**, and naked crystal upon exposure to a saturated environment of toluene (0.037 atm).

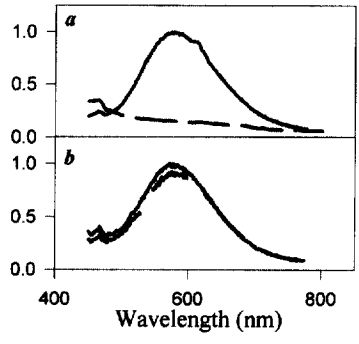

Fig. 12. Thin film photoluminescence: (a) nitrobenzene (3.0×10^{-4} atm) exposure of square **2**, and (b) toluene (0.037 atm) exposure of square **2** for 1 min.

transfer with the photoexcited form of **2**, thereby oxidatively quenching its emission. The ability in Fig. 12 to distinguish between chemically and sterically similar guests that are essentially indistinguishable by QCM measurements suggests that thin film photoluminescence may prove useful in enhancing the chemical selectivity of metallocyclophane-based sensing devices.

7. Conclusions

A new class of inorganic cyclophanes has been synthesized which introduces octahedral transition-metal centers directly into the corners of square frameworks. The *fac*-$Re(CO)_3(\mu\text{-imine})_2Cl$ corners are capable of forming luminescent excited states (MLCT excited states) following visible region excitation. When dipyridyl

porphyrin ligands are employed as edges, however, the luminescence observed is that of the porphyrin. The ability to control the size and chemical composition of the squares has permitted them to function in solution as moderately chemically selective hosts for both complex anion guests and a representative diimine guest, where host:guest binding has been followed via light emission.

Nanoporous solid films of these square assemblies have been used in luminescence, microgravimetric (QCM), and electrochemical sieving (RDE) studies. These studies suggest that the ability to tune the cavity sizes of the component molecular squares, together with the tendency of the squares to form elongated channels in the solid state, will permit the corresponding thin film materials to be used in a variety of small molecule sieving applications wherein the exclusion limit can be altered by altering the dimensions of the square [60–62]. Finally, the variable luminescence responses of nanoporous films to selected volatile organic compounds implies that the films can be exploited in chemical sensing devices to differentiate between compounds/analytes of similar shape and size (e.g. nitrobenzene and toluene).

Acknowledgements

We gratefully acknowledge the donors to the Petroleum Research Fund, administered by the American Chemical Society, and the US Geological Survey (Illinois Water Resources Center) for support of this research. We also thank the NSF (Grant No. CHE-9303682) for preliminary support. RVS additionally thanks the NSF for predoctoral fellowship support. SB thanks the Fonds FCAR for postdoctoral fellowship support.

References

[1] W.C. Kalb, Z. Demidowicz, D.M. Speckman, C. Knobler, R.G. Teller, M.F. Hawthorne, Inorg. Chem. 21 (1982) 4027.
[2] P.M. Stricklen, E.J. Volcko, J.G. Verkade, J. Am. Chem. Soc. 105 (1983) 2494.
[3] M. Fujita, J. Yazaki, K. Ogura, J. Am. Chem. Soc. 112 (1990) 5645.
[4] M. Fujita, O. Sasaki, T. Mitsuhashi, T. Fujita, J. Yazaki, K. Yamaguchi, K. Ogura, J. Chem. Soc., Chem. Commun. (1996) 1535.
[5] M. Fujita, J. Yazaki, K. Ogura, Tetrahedron Lett. (1991) 5589.
[6] M. Fujita, S. Nagao, M. Iida, K. Ogata, K. Ogura, J. Am. Chem. Soc. 115 (1993) 1574.
[7] M. Fujita, F. Ibukuro, H. Hagihara, K. Ogura, Nature 367 (1994) 720.
[8] H. Rauter, E.C. Hillgeris, A. Erxleben, B. Lippert, J. Am. Chem. Soc. 116 (1994) 616.
[9] P.J. Stang, D.H. Cao, J. Am. Chem. Soc. 116 (1994) 4981.
[10] P.J. Stang, B. Olenyuk, J. Fan, A.M. Arif, Organometallics 15 (1996) 904.
[11] V.V. Zhdanki, P.J. Stang, J. Am. Chem. Soc. 115 (1993) 9808.
[12] P.J. Stang, D.H. Cao, S. Saito, A.M. Arif, J. Am. Chem. Soc. 117 (1995) 6273.
[13] P.J. Stang, B. Olenyuk, Angew. Chem., Int. Ed. Engl. 35 (1996) 732.
[14] C.M. Drain, J.-M. Lehn, J. Chem. Soc., Chem. Commun. (1994) 2313.
[15] R.V. Slone, D.I. Yoon, R.M. Calhoun, J.T. Hupp, J. Am. Chem. Soc. 117 (1995) 11813.
[16] R.V. Slone, J.T. Hupp, C.L. Stern, T.E. Albrecht-Schmitt, Inorg. Chem. 35 (1996) 4096.
[17] R.V. Slone, J.T. Hupp, Inorg. Chem. 36 (1997) 5422.

[18] D.B. Macqueen, K.S. Schanze, J. Am. Chem. Soc. 113 (1991) 6108.
[19] Y. Shen, B.P. Sullivan, J. Chem. Ed. 74 (1997) 685.
[20] M.S. Wrighton, P.J. Giordano, J. Am. Chem. Soc. 101 (1979) 2888.
[21] G.A. Lawrance, Chem. Rev. 86 (1986) 17.
[22] C. Diver, G.A. Lawrance, J. Chem. Soc., Dalton. Trans. (1988) 931.
[23] A.P. Sanger, J. Chem. Soc., Dalton Trans. (1977) 1971.
[24] R.V. Slone, J.T. Hupp, I.A. Guzei, A.L. Rheingold, unpublished results.
[25] F. Vögtle, P. Neumann, Synthesis (1973) 85.
[26] P.M. Keehn, S.M. Resenfeld (Eds.), Cyclophanes, Academic Press, New York, 1983.
[27] D.S. Lawrence, T. Jiang, M. Levett, Chem. Rev. 95 (1995) 2229.
[28] X. Chi, A.J. Guerin, R.A. Haycock, C.A. Hunter, L.D. Sarson, J. Chem. Soc., Chem. Commun. (1995) 2563.
[29] X. Chi, A.J. Guerin, R.A. Haycock, C.A. Hunter, L.D. Sarson, J. Chem. Soc., Chem. Commun. (1995) 2567.
[30] F. Zingales, U. Sartorelli, A. Trovati, Inorg. Chem. 6 (1967) 1246.
[31] F. Zingales, M. Graziani, F. Faraone, U. Belluco, Inorg. Chim. Acta 1 (1967) 172.
[32] K. Kalyanasundaram, Photochemistry of Polypyridine and Porphyrin Complexes, Academic Press, London, 1992.
[33] J. Lees, Chem. Rev. 87 (1987) 711.
[34] T.J. Meyer, Pure Appl. Chem. 58 (1986) 1193.
[35] G. Tapolsky, R. Duesing, T.J. Meyer, Inorg. Chem. 29 (1990) 2285.
[36] J.V. Caspar, T.J. Meyer, J. Phys. Chem. 87 (1983) 952.
[37] R. Engleman, J. Jortner, Mol. Phys. 18 (1970) 145.
[38] P. Avouris, W.M. Gelbart, M.A. El-Sayed, Chem. Rev. 77 (1977) 793.
[39] D.I. Yoon, C.A. Berg-Brennan, H. Lu, J.T. Hupp, Inorg. Chem. 31 (1992) 3192.
[40] J.V. Caspar, Ph.D. Dissertation, The University of North Carolina, 1982.
[41] R.E. Dale, J. Eisinger, Biopolymers 13 (1974) 1573.
[42] A. Gilbert, J. Baggott, Essentials of Molecular Photochemistry, CRC Press, Boston, 1991, p. 91.
[43] B. Grossman, J. Heinze, E. Herdtweck, F.H. Köhler, H. Nöth, H. Schwenck, M. Spiegler, W. Wachter, B. Weber, Angew. Chem., Int. Ed. Engl. 36 (1997) 387.
[44] V. Balzani, F. Bolletta, M.T. Gandolfi, M. Maestri, Top. Curr. Chem. 75 (1978) 1.
[45] M.D. Todd, Y. Dong, J. Horney, D.I. Yoon, J.T. Hupp, Inorg. Chem. 32 (1993) 2001.
[46] S. Anderson, H.L. Anderson, A. Bashall, M. McPartlin, J.K.M. Sanders, Angew. Chem., Int. Ed. Engl. 34 (1994) 1096.
[47] E.B. Fleischer, A.M. Schachter, Inorg. Chem. 30 (1991) 3763.
[48] J.R. Miller, G.D. Dorough, J. Am. Chem. Soc. 74 (1952) 3977.
[49] M. Fujita, Y.J. Kwon, S. Washizu, K. Ogura, J. Am. Chem. Soc. 116 (1994) 1151.
[50] M. Fujita, Y.J. Kwon, O. Sasaki, K. Yamaguchi, K. Ogura, J. Am. Chem. Soc. 117 (1995) 7287.
[51] L. Carlucci, G. Ciani, D.M. Proserpio, A. Sironi, J. Chem. Soc., Chem. Commun. (1990) 2755.
[52] L.R. MacGillivray, S. Subramanian, M.J. Zaworotko, J. Chem. Soc., Chem. Commun. (1994) 1325.
[53] R.W. Gable, B.F. Hoskins, R. Robson, J. Chem. Soc., Chem. Commun. (1990) 1677.
[54] F.L. Dickert, A. Haunschild, V. Kuschow, M. Reif, H. Stathopulos, Anal. Chem. 68 (1996) 1058.
[55] F.L. Dickert, M. Reif, H. Reif, Fresenius J. Anal. Chem. 352 (1995) 620.
[56] C.S.I. Lai, G.J. Moody, J.D.R. Thomas, D.C. Mulligan, J.F. Stoddart, R. Zarzycki, J. Chem. Soc., Perkin Trans. 2 (1988) 319.
[57] J.W. Grate, S.J. Patrash, M.H. Abraham, Anal. Chem. 67 (1995) 2162.
[58] J.W. Grate, S.J. Patrash, Anal. Chem. 68 (1996) 913.
[59] K.D. Schierbaum, T. Weiss, E.U.T. van Velzen, J.F.J. Engbersen, D.N. Reinhoudt, W. Göpel, Science 265 (1994) 1413.
[60] W.-J. Chen, P. Aranda, C.R. Martin, J. Membr. Sci. 107 (1995) 199.
[61] W.-J. Chen, C.R. Martin, J. Membr. Sci. 104 (1995) 101.
[62] C.R. Martin, Science 266 (1994) 1961.